ACS OMEGA

http://pubs.acs.org/journal/acsodf
Article

Combined Thermomechanical Effect of Graphene Oxide and Montmorillonite on Biobased Epoxy Network Formation for Coatings

Mădălina Ioana Necolau, Brînduşa Bălănucă, Adriana Nicoleta Frone, Iulia Nicoleta Radu, Graţiela Grădişteanu-Pîrcălăbioru, and Celina Maria Damian*

Cite This: ACS Omega 2024, 9, 8297−8307
Read Online

ABSTRACT: Epoxy nanocomposites derived from linseed oil, reinforced with graphene oxide (GO) and montmorillonite (MMT) nanostructures, were synthesized. The nanohybrids were developed by enriching the structure of MMT and GO with primary amines through a common and simplified method, which implies physical interactions promoted by ultrasonic processing energy. The influence of the new nanoreinforcing agents along with neat ones on the overall properties of the biobased epoxy materials for coating applications was assessed. Interface formation through surface compatibility was contained by the lower values of activation energy calculated from differential scanning calorimetry (DSC) curves, along with a consistent 70% increase in the cross-linking density when amine-modified MMT was used. Thermomechanical characteristics of the biobased epoxy nanocomposites were explained through the interaction of the functional groups over the curing process of epoxidized linseed oil (ELO), giving a 15 °C higher T_g value increase. Furthermore, the low surface energy values suggested an intrinsic antibacterial activity, as proved by a significant decrease of CFU against *Staphylococcus aureus* bacterial strains on the 0.25% reinforced coatings.

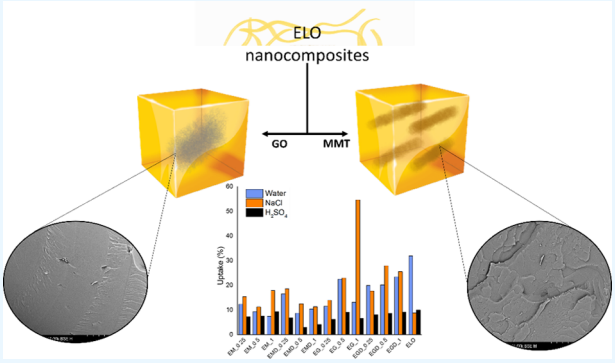

1. INTRODUCTION

Epoxy resins represent a significant class of thermosets with large applicability in high-tech industries such as automotive, aerospace, and electronics due to their superior mechanical strength, good thermostability, and excellent adhesion to a variety of substrates.[1−3]

The progressive evolution encountered in the technological field has enforced the development of new advanced polymeric composites through the incorporation of nanosized particles into the epoxy matrix to achieve improved performances.[4,5]

Graphene oxide (GO) has generated a lot of interest owing to its superior thermal, electrical, and mechanical properties.[6] Moreover, the planar geometry decorated with polar functionalities and a high specific surface area[7,8] make GO an ideal candidate for the development of high-performance nanocomposite materials through tailoring the polymer−filler adhesion by functionalization.[9−11]

The association of nanoclays with polymers to produce nanocomposites is another method to tune the performance.[12,13] Designed properties such as thermal stability and mechanical properties can be considerably improved only by the inclusion of <5% weight nanoclays into the neat polymer.[14]

Natural oils represent an abundant resource for this purpose with tremendous potential as chemical feedstock. Soybean oil is the most used plant oil, and it is mainly harvested within the USA. Triglycerides from vegetable oils contain various fatty acids, such as linoleic, linolenic, oleic, palmitic, and stearic acid. These fatty acids have different chain lengths, compositions, and distributions, as can be observed from Table 1.[15] By considering linseed and tung oil with the 18:3 ratio containing fatty acids, studies showed a better rate of oxidation for the conjugated α-eleostearic acid from tung oil,[16] while the major disadvantage is its wrinkle formation upon drying.[17] The polymer networks formed by this oil are rigid and brittle. On the other hand, due to its favorable composition, linseed oil leads to epoxy networks with a higher tensile strength and modulus compared with castor oil-based epoxies, while the thermal properties of epoxy networks resulting from both castor and linseed oils were similar to conventional epoxy resins.[18]

Received: November 14, 2023
Revised: December 30, 2023
Accepted: January 5, 2024
Published: February 9, 2024

https://doi.org/10.1021/acsomega.3c09059
ACS Omega 2024, 9, 8297−8307

Table 1. Fatty Acid Composition for Different Vegetable Oils

vegetable oil	fatty acid				
	linoleic (18:2)	linolenic (18:3)	oleic (18:1)	palmitic (16:0)	other
linseed	17	52	22	6	3
soybean	53	7	24	12	4
tung	6	3	8	2	81[a]
castor	4.7	0.7	3.3	1.1	90.2[b]

[a]Mostly α-eleostearic acid (*cis*, *trans*, *trans*-triply conjugated). [b]Mostly ricinoleic acid.

When structurally converted into polymeric compounds, vegetable oils do not exhibit high rigidity and mechanical properties that are required for structural applications. Therefore, numerous studies have been reported along time regarding the synthesis of green nanocomposites based on vegetable oil epoxy networks derived from linseed,[19] soybean,[20] tung,[21] and castor[22] oils and reinforced with different nanostructures such as GO,[23] multiwalled carbon nanotubes (MWCNTs),[24] polyhedral oligomeric silsesquioxanes (POSSs),[25] and nanoclays[26] for applications in various fields.

However, research on GO- and nanoclay-reinforced epoxidized linseed oil is quite limited, and the influence of these nanostructures needs to be comprehensively evaluated. Hegde et al.[27] synthesized nanocomposite coatings based on epoxidized linseed oil reinforced with reduced graphene oxide (rGO) for anticorrosive applications and observed that the synthesized materials exhibited 99.98% efficiency against corrosion of mild steel and also decreased the rate of corrosion by 5000 times. Apart from that, rGO nanofillers significantly contributed to the thermal properties.

Herein, the present study proposes the development of biodegradable epoxy nanocomposite materials in which the influence of graphene oxide and montmorillonite as reinforcing agents was analyzed in terms of thermal and mechanical properties.

2. EXPERIMENTAL SECTION

2.1. Materials Used within This Study. The GO structures were synthesized by our team through a modified Hummers method and reported elsewhere. Methanol and acetone were purchased from Sigma-Aldrich. Polyetheramine Jeffamine D230 was kindly provided by Huntsman. Natural sodium montmorillonite (MMT) Nanofil 116 with a cation exchange capacity (CEC) of 116 mequiv/100 g of clay was purchased from Southern Clay Products. The epoxidized linseed oil (ELO) used in this study was previously synthesized and characterized by Balanuca et al.[28] To cross-link the biobased epoxy matrix, citric acid monohydrate (>99.5%) from Alfa Aesar was used in the presence of anhydrous THF (≥99.9%, inhibitor-free) from Sigma-Aldrich.

2.2. Nanofillers. Nanofiller structures were modified through functionalization with D230 polyetheramine by a method described previously.[29] In short, GO layers were exfoliated by using the ultrasonication energy from a tip sonicator. For GD synthesis, an amount of 1 mg/mL suspension of GO in ethanol was obtained, and then a 1% solution of D230 in ethanol was added and then sonicated for one more hour. The MMTD nanohybrids were synthesized through an organophilization process by swelling in water at 80 °C for 1 h, and then similar to GD, they were mixed with 1 mg/mL HCl-protonated D230 solution under sonication.

2.3. Nanocomposites. Nanocomposites were synthesized following specific steps: the calculated ratio of nanofillers (0.25, 0.5, and 1 wt %) was dispersed in the polymeric matrix for 15 min by using a probe ultrasonicator with a frequency of 100 kHz and an amplitude of 40%. The cure reaction was done by solubilizing a stoichiometric amount of citric acid (considering the molar ratio of COOH and epoxy groups in the epoxidized oil structure) in THF at 80 °C, followed by addition to the ELO−nanofiller suspension. After slight gel formation, for about 5 min at 80 °C, the reaction mixture was placed in a Teflon mold and subjected to thermal curing for 3 h at 80 °C, 1 h at 100 °C, and 1 h at 150 °C. The composition of each sample along with the abbreviations is presented in Table 2.

Table 2. Biobased Epoxy Nanocomposite Sample Composition and Abbreviations

sample	ratio (%)	abbreviation	
ELO matrix		ELO	
ELO-GO	0.25	EG	EG_0.25
	0.5		EG_0.5
	1		EG_1
ELO-GOD	0.25	EGD	EGD_0.25
	0.5		EGD_0.5
	1		EGD_1
ELO-MMT	0.25	EM	EM_0.25
	0.5		EM_0.5
	1		EM_1
ELO-MMTD	0.25	EMD	EMD_0.25
	0.5		EMD_0.5
	1		EMD_1

2.4. Characterization. Differential scanning calorimetry (DSC) curves were recorded on a Netzsch DSC 204 F1 Phoenix equipment. The measurements were conducted at heating rates of 5, 10, 15, and 20 °C/min under a nitrogen atmosphere (20 mL/min flow rate) from RT to 300 °C.

The apparent activation energy (E_a) of the curing reaction was computed with the aid of Kissinger[30] (eq 1) and Ozawa[31] (eq 2) equations:

$$\ln\left(\frac{\beta}{T_p^2}\right) = \ln\frac{AR}{E_a} - \frac{E_a}{RT_p} \quad (1)$$

$$\ln\beta = -1.052E_aRT_p + C \quad (2)$$

where β is the heating rate (°C/min); T_p is the maximum temperature of the polymerization peak (K); A is the pre-exponential factor; R is the gas constant (R = 8.314 J/mol·K); E_a is the activation energy (kJ/mol); and C is a constant.

Thermogravimetric analysis (TGA) was performed using a Netzsch TG 209 F1 Libra equipment, under a nitrogen and synthetic air atmosphere from RT to 800 °C with a heating rate of 10 °C/min.

Dynamic mechanical analysis (DMA) tests were conducted on a TRITEC 2000 B equipment with a heating rate of 4 °C/min in single cantilever bending mode at 1 Hz frequency in the temperature range of −90 to 100 °C. Based on the DMA results, the cross-linking density (υ_e) was calculated for each studied system using the following equation:[32]

https://doi.org/10.1021/acsomega.3c09059
ACS Omega 2024, 9, 8297−8307

$$v_e = E'/3RT \quad (3)$$

where E' is the storage modulus in the rubbery region at $T = T_g + 30$ and T and R correspond to the absolute temperature (K) and the ideal gas constant, respectively.

Contact angle (CA) measurements were conducted using the drop shape analyzer-DSA100 from Krüss Scientific GmbH through a sessile drop method at room temperature using water and ethylene glycol as the polar and nonpolar probing liquids. Analysis was performed by deposition of a solvent droplet with a volume of 2 μL, which was maintained for 10 s on the sample surface. The contact angle values were determined using the Young−Laplace equation in Advance software by registering 10 frames/s and representing the average values for each sample. The determination of surface free energies was calculated in the same software using the Young−Dupré and Fowkes equations, which considered the polar work of adhesion and the corresponding surface tensions of the liquids used for analysis.

The contact angle was determined by using the Young−Laplace fitting method equation in Advance software and it represents the average of three measurements for each sample.

Samples were analyzed for the water absorption (WA) degree following a procedure described in the ASTM D570 standard; also, the method was performed in triplicate determination for each ELO-based material for an accurate result.

The fracture morphology of the nanocomposites was also analyzed by scanning electron microscopy (SEM). The samples were coated with a gold conductive layer by sputtering, and further, the images were recorded using a Quanta 200 environmental scanning electron microscope (FEI-Philips) with a tungsten electron source, in low vacuum mode, at an accelerating voltage of 30 kV.

3. RESULTS AND DISCUSSION

3.1. Structural Characterization. The raw GO and MMT nanomaterials used as reinforcing agents in the epoxidized linseed oil networks were extensively characterized from structural and thermal points of view in our previous study.[29] Thus, the crystallites were observed through XRD in order to assess the interplanar distances from specific diffraction peaks, giving a 3.6 nm value for GO-layered nanosheets. From the Scherrer equation used to estimate the nanocrystallite size using XRD data, the GO dimensions correspond to particles which can contain between 6 and 7 sheets, while GOD nanostructures are lower in dimensions up to 5 sheets.

By analyzing the Raman spectra represented in Figure 1, it can be observed that the main characteristic peaks of graphene-type nanostructures are present: the D band ascribed to the electronic defects induced within the extended aromatic feature, the G band given by the condensed graphite-type aromatic structure, and the 2D band which arises from the second-order two-phonon processes similar to the G band; however, this one is more sensitive to the laser particularities. There is valuable information which can be extracted from the Raman spectra: on one hand, the intensity ratio for the main characteristic bandsI_D/I_G whose value increases from 0.748 for GO to 0.777 for GOD, revealing a defect induced by the attachment of amine molecules to the GO structures. The second data is disposed through the shifting of the G band position from 1580 cm^{-1} for GO to 1588 cm^{-1} for GOD, which shows a decrease in the number of graphene oxide layers

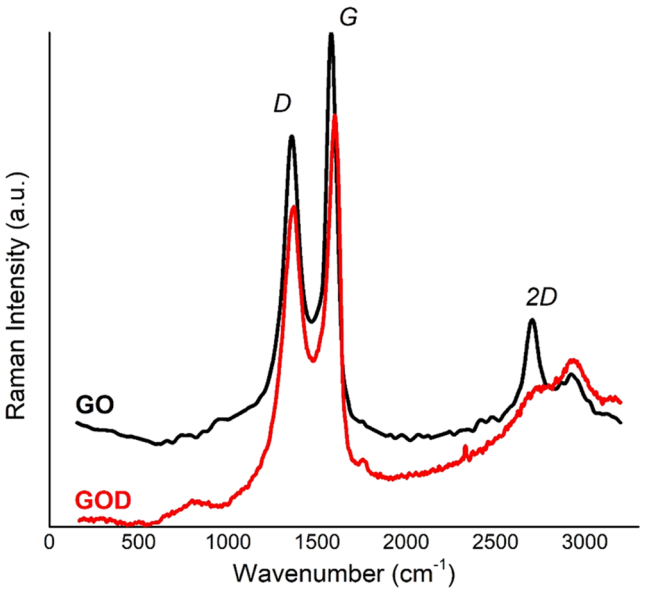

Figure 1. Raman spectra for the graphene oxide structures.

in the GOD crystallites, as previously calculated from XRD data. Although the shape of the 2D band could also give a hint on the number of layers in GO nanostructures, according to this feature, the GOD spectra shows graphite-like alure. These data are not consistent with XRD and the G band position, probably because of the sensitivity of the 2D band mentioned above.

3.2. Curing Behavior of Biobased Networks. The energy exchange monitored through the nonisothermal DSC thermograms and the corresponding parameters given in Table 3 provides valuable information on the curing reaction

Table 3. Thermal Characteristics Calculated for the Cure Reaction of ELO-Based Materials

sample	ratio (%)	ΔH (J/g)	T_{max}	E_a (kJ/mol), Kissinger	E_a (kJ/mol), Ozawa
E		174.1	108.0	53.52	57.13
EG	0.25	193.8	117.2	63.29	66.53
	0.5	149.3	116.6	68.55	71.52
	1	151.6	116.1	80.07	82.44
EGD	0.25	234.6	104.6	47.66	51.51
	0.5	193.5	111.2	50.20	54.03
	1	215.7	105.7	47.98	51.84
EM	0.25	102.5	111.4	58.05	61.47
	0.5	145.4	118.1	73.31	76.02
	1	158.0	116.4	61.14	67.40
EMD	0.25	248.9	109.8	46.49	50.49
	0.5	231.2	117.4	74.43	77.09
	1	252.2	108.0	43.79	47.91

mechanism of the ELO monomer in the presence of GO and MMT. Analyzing the curves from Figure 2, one can observe that there is a significant influence of the nano-reinforcing agents over the curing profiles of the biobased nanocomposites. Thus, in the first stage of thermal treatment, the curing enthalpy showed higher values for EG_0.25 nanocomposites, while EM_0.25 determined a lower value, possibly due to a hindrance effect induced by the morphology of the layered clay. Analyzing the enthalpy for the EGD and EMD samples, a significant increase in the evolved heat was

https://doi.org/10.1021/acsomega.3c09059
ACS Omega 2024, 9, 8297−8307

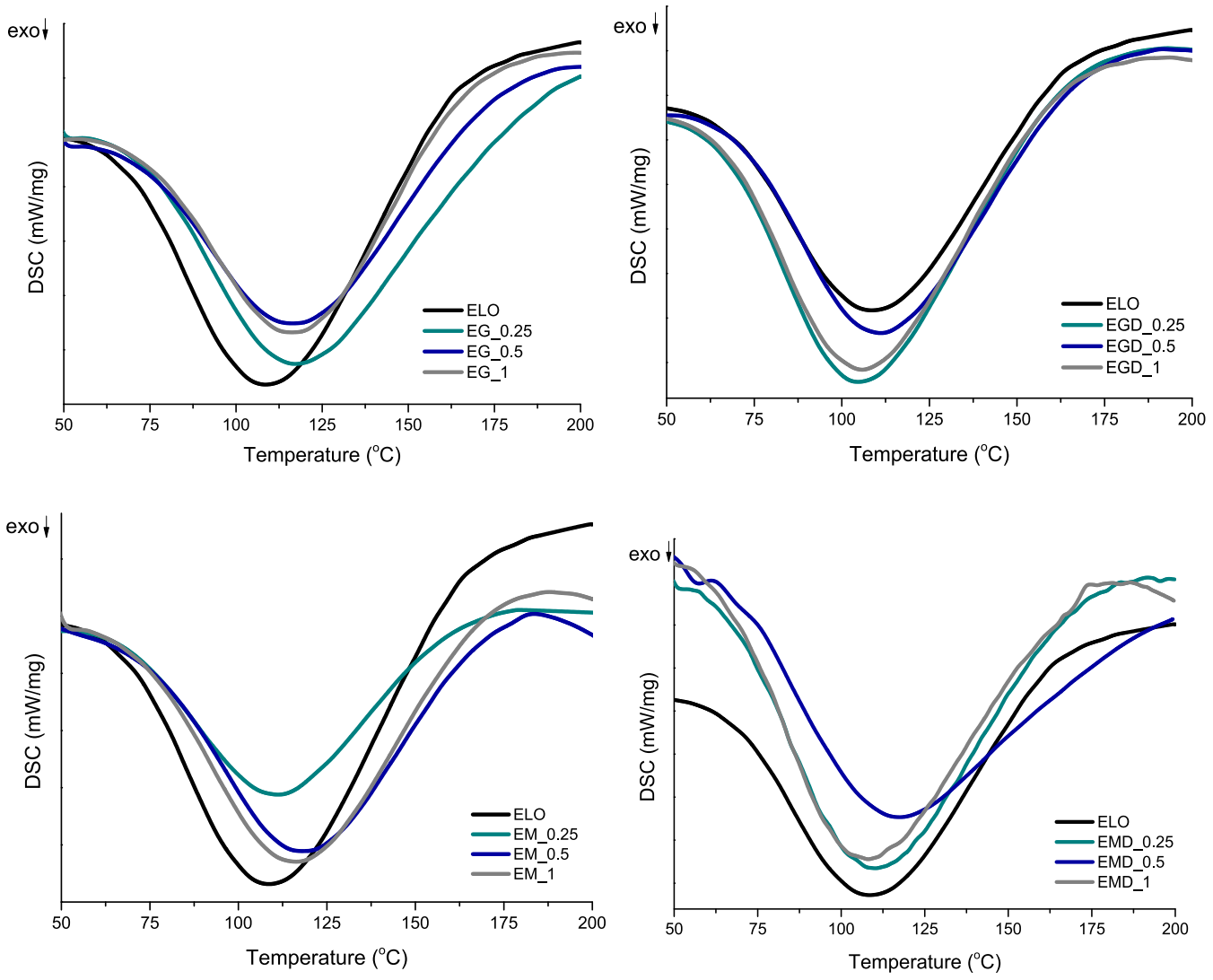

Figure 2. DSC profiles for ELO-based nanocomposite networks.

observed, and it can be ascribed to the supplementary interactions developed between the primary amine groups grafted onto the nanoreinforcing agents after functionalization with D230 and the polymeric matrix. In this case, a synergistic influence of the nanohybrid material over the curing process can be considered. The NH_2 groups from the nanostructures will lead to epoxy ring opening prior to network formation, which is translated as an increased ΔH, while the resulting OH groups can interact by creating the ester-type network (in the prepolymer/oligomers) with the curing agent.

The activation energy (E_a) calculated for the analyzed bioepoxy systems using Kissinger and Ozawa methods represents a valuable parameter which defines the thermal behavior of the complex nanocomposite systems. In this context, the lower values of the E_a for EMD_0.25 and EGD_0.25 connected with the higher ΔH values highlight the above-mentioned hypothesis. The compatibility between the oil-based monomer and the reinforcing agent can be translated into the E_a value, knowing that higher values for this parameter denotes a reduced interaction between the components of the system.[33] Based on the E_a values listed in Table 3 for EG and EM systems, it can be seen that unfunctionalized GO and MMT exert limited interactions with the ELO matrix. Thus, a general tendency of a higher temperature at which the reaction rate has the maximum value (T_{max}) is noticed along with the addition of GO and MMT. However, GD is acting like a catalyst in accordance with the hypothesis by which NH_2 is reacting in the first stage with the epoxy groups from ELO structures; in this case, the additional amine functionalities have a significant contribution over the curing process.

3.3. Thermomechanical Features of ELO Nanocomposites. The influence of the nanofillers over the viscoelastic performances of biobased epoxy networks was evaluated through dynamic mechanical analysis (DMA). The E' values at room temperature (25 °C), glass transition temperature (T_g), and cross-linking density are collectively presented in Table 3.

The overall viscoelastic response of the nanocomposites resembles that of the conventional thermoset amorphous polymers, displaying a drop in modulus in the proximity of the glass transition due to the enhanced chain mobility generated by this phase transition.

As can be observed from Figure 3 (the inset of tan δ), the glass transition of ELO samples takes place between 20 and 50 °C. Among the nanocomposite samples, only the ones with MMT reinforcement present an early transition, probably due

https://doi.org/10.1021/acsomega.3c09059
ACS Omega 2024, 9, 8297−8307

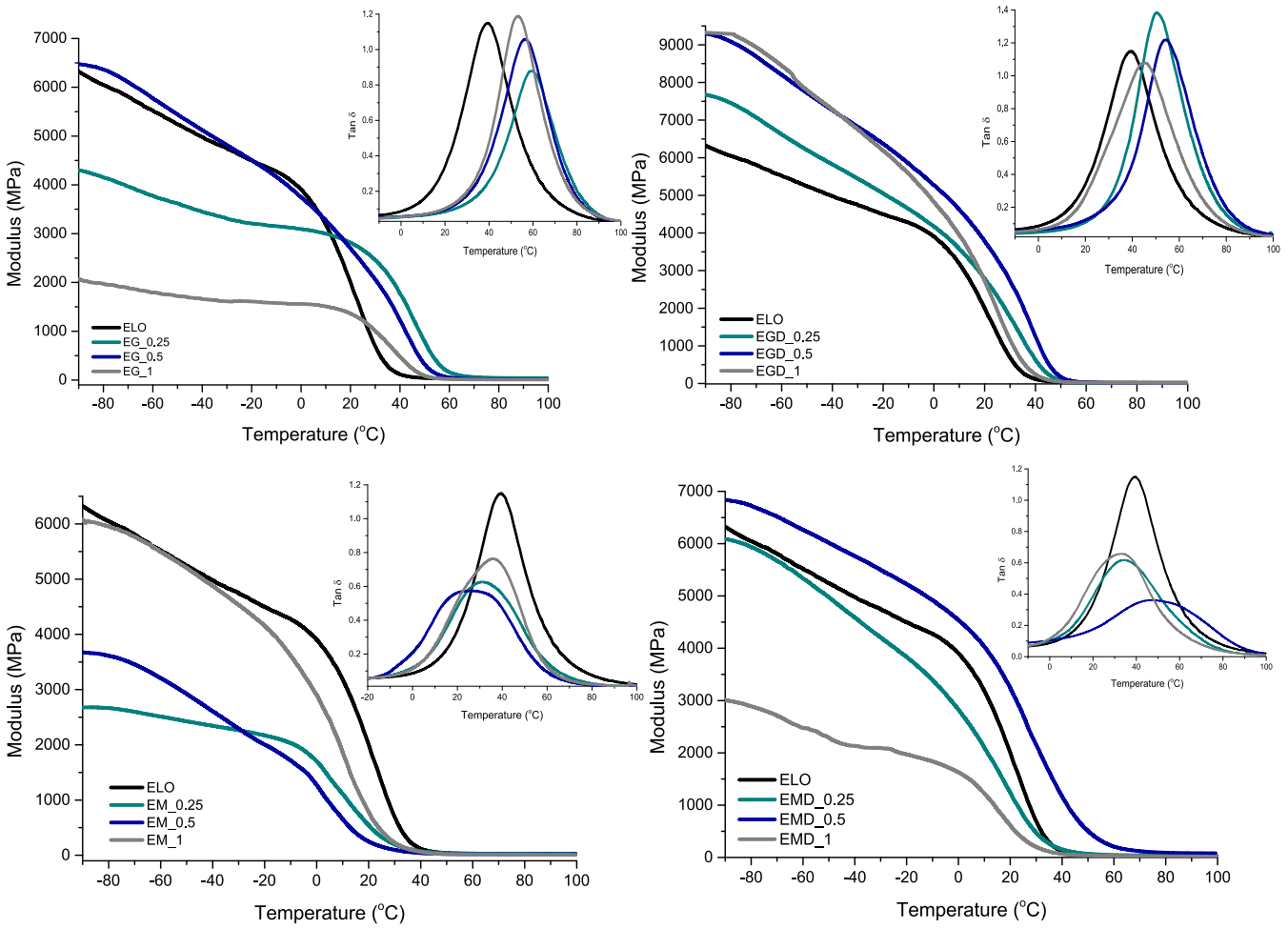

Figure 3. Storage modulus and tan δ curves obtained from DMA analysis for ELO-based nanocomposites.

to an incompatibility at the interface that leads to the agglomeration of the nanoclay that will further hinder the curing agent to reach the reactive sites at a higher concentration, thus resulting in an excess of triglyceride unbonded into the matrix, which will act as an internal plasticizer. However, 0.25% MMT showed an increased cross-linking density than the ELO matrix, which means that at a low concentration, it is possible for the cross-linking process to take place more efficiently despite the incompatibility of the components.

The incorporation of 0.25 and 0.5% GO and GOD significantly improved the T_g and the E' value of the ELO composite, mostly in the viscoelastic and rubbery regions, having values between 1900 and 3300 MPa at 25 °C, an increment of 2-fold as compared to the matrix. These values highlight the good reinforcing capacity of the carbonaceous structures along with a good interaction between them and the polymeric matrix.[34,35]

The tan δ curve width is an indicator for the structural homogeneity within the epoxy networks, while the intensity of the loss factor peak conveys the chain segment mobility of a polymer network at relaxation temperature. This peak widening shows that the glass transition of nanocomposites takes place over a wide range of temperature, as similar data was also reported in the case of CNT addition to the ELO/PANI5 matrix[35] or in the case of polyamide-6/HNT samples.[36] The nanocomposite samples with MMT-based reinforcing agents express the most notable tan δ expanding, which is in accordance with the DSC data.

When looking at the CD values presented in Table 4, we can conclude that at a lower concentration of nanostructures (0.25%), the overall values for the corresponding nanocomposites are higher as compared with those of the neat ELO matrix, except for the EGD nanocomposite. This is contrary to the hypothesis that the NH_2 groups will be

Table 4. Thermomechanical Parameters of ELO-Based Materials Obtained from the DMA Tests

sample	ratio (%)	E' at 25 °C (MPa)	T_g (deg)	cross-linking density (mol/cm^3)
E		1327.1	38.5	3089
EG	0.25	2671.9	58.5	4677
	0.5	2394.1	55.8	1891
	1	1231.9	52.1	1206
EGD	0.25	2318.4	49.4	1370
	0.5	3304.1	53.5	1274
	1	1952.4	44.6	2066
EM	0.25	317.2	28.8	3725
	0.5	147.2	26.6	2435
	1	444.7	35.0	1858
EMD	0.25	825.6	32.8	5278
	0.5	2730.8	45.4	1169
	1	387.2	31.3	3691

https://doi.org/10.1021/acsomega.3c09059
ACS Omega 2024, 9, 8297−8307

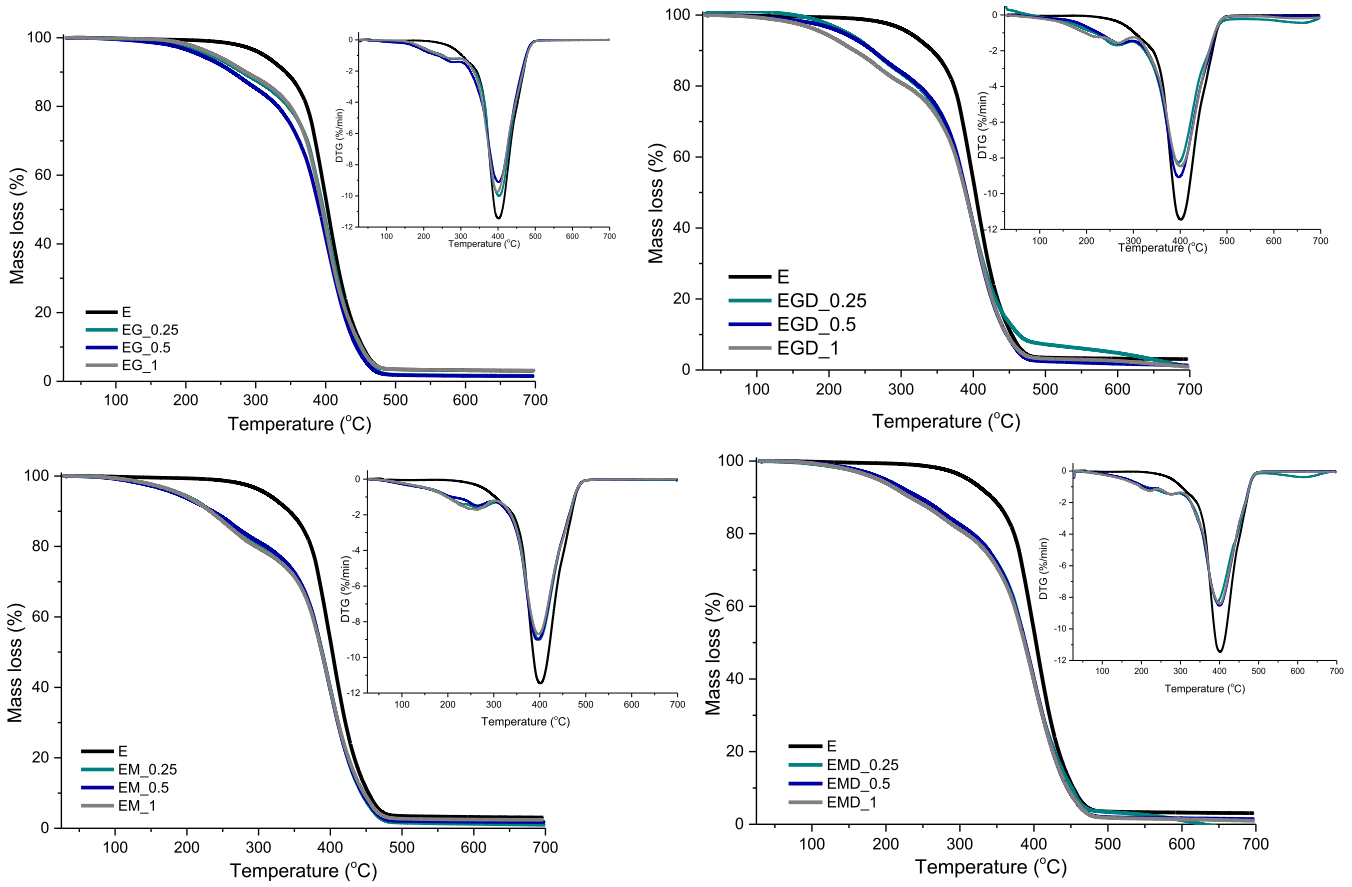

Figure 4. Thermal behavior of ELO and ELO nanocomposites based on (a) GO, (b) GOD, (c) MMT, and (d) MMTD.

Table 5. Thermal Data for the ELO Networks and the Resulting Nanocomposites in Inert and Oxidative Medium

sample	report (%)	$T_{d3\%}$ (deg)	$T_{d3\%}$ (deg) air	T_{max} (deg)		T_{max} (deg) air		residual mass (%)	residual mass (%) air
E		290.3		401.7				3.07	
EG	0.25	206.6	201.6	402.4	402.4	522.5		1.62	1.60
	0.5	194.1	195.0	401.5	399.2	540.1		1.52	0.91
	1	218.1	199.2	397.5	403.1	535.2		3.15	2.16
EGD	0.25	203.8	187.1	396.0	271.0	415.0	533.0	1.13	0.67
	0.5	192.2	182.5	396.0	277.1	414.5	538.3	1.26	0.81
	1	166.2	192.8	403.0	274.3	411.5	509.0	0.90	1.08
EM	0.25	160.8	178.8	397.5		419.3	536.0	0.99	1.33
	0.5	154.7	178.1	393.6	377.3	413.7	526.6	1.76	1.18
	1	163.0	195.9	396.5	376.9	414.4	520.2	2.41	2.47
EMD	0.25	164.7	174.6	394.3	405.1		531.3	1.22	0.90
	0.5	171.1	171.1	400.6	400.6			1.42	1.42
	1	161.5	161.5	398.9	400.7			0.95	0.95

involved in the epoxy ring opening, thus increasing the cross-linking density. This means that there may be some concurrent reactions between the functional groups present on the basal plane of GO. On one hand, OH groups from unfunctionalized GO can enhance the CD through interactions with COOH groups from citric acid to provide more active H that will further enhance the curing reaction yield. On the other hand, although NH_2 groups are involved in epoxy network formation at lower concentrations, as can be seen from the T_{max} and E_a values from Table 3, the CD values are much lower in this case, which can be explained by the hindering effect of the large GD structures over AC mobility during the curing reaction. This phenomenon may be due to the fact that the physical properties of the polymer adjacent to the nanofiller are varying from the ones of the matrix, also suggesting a high interfacial area between the two components of the nanomaterial.[37]

3.4. Thermal Stability of the ELO Nanocomposite Materials. Thermostability and degradation profiles of the biobased epoxy nanocomposites were investigated by TGA under a nitrogen atmosphere, and the resulting thermograms are depicted in Figure 4. The onset of thermal degradation was considered the temperature at 3% of mass loss ($T_{d3\%}$). The thermal degradation process mainly demonstrates a single mass-loss stage between 300 and 500 °C, corresponding to the cleavage of the ELO chains. The nanocomposite materials disclose an additional degradation step that occurs between

https://doi.org/10.1021/acsomega.3c09059
ACS Omega 2024, 9, 8297−8307

150 and 300 °C that may be assigned to the presence of multiple oxygenated functionalities or atoms on both types of nanoreinforcing agents, namely, GO structures and MMT clay.

Considering the significant decrease of $T_{d3\%}$ values, as shown in Table 5, the influence comes from the interphase epoxy network (defined as the volume of the matrix which interacts with the surface of the nanoreinforcing agents). This is done through functional groups as well as the contact surface area.[38,39] When looking at the mass loss of nanocomposite samples at 290 °C, which is the onset degradation of the matrix, the obtained values can be connected to the presence of oxygen-containing groups from GO and MMT, which can generate more initial degradation active centers, leading to lower onset values for thermal alteration of the nanocomposites. This theory is also supported by the lower char yield values registered for the nanocomposite materials.

This aspect demonstrates that the nanoparticles dispersed through the macromolecular biobased epoxy chains can modify the degradation mechanism of the network, as the epoxy interphase is highly affected by the reciprocal action promoted by the functionalities from the nanoreinforcing agents. Although the nanoreinforcing agents are influencing the topochemistry of the networks through their surface functional groups, they are not altering the overall thermal performance, as can be observed in the inset curves of DTG. Moreover, this aspect is cleared by nanocomposite analysis in an oxidative atmosphere, which shows a supplementary degradation step at lower temperatures assigned to the interphase decomposition mostly visible for the EGD and EM samples (TGA and DTG curves are supplied as Figures S1 and S2), and one step at higher temperatures that is coming from the final cyclization and aromatization of the char.

However, the char residual mass of the EG and EGM nanocomposites at 600 °C underwent a slight increase in the case of 1% nanocomposites. Such an effect could be attributed to the formation of a thermally stable protective layer that prevented the decomposition of the polymeric matrix underneath it. This mechanism was also reported by Mendes et al. for an AESO-based system reinforced with 0.5 wt % acr-RGO, which obtained an increased char yield from 1.2 wt % at 600 °C to 3.5 wt % for added 1% acr-RGO;[40] in our case, the functionalities are more numerous, considering the starting GO respectively MMT, and thus a slight increase is observed.

3.5. Surface Characteristics. Contact angle (CA) measurement is an important aspect to characterize biobased materials for coating applications, in terms of wettability, surface free energy, or adhesion to different substrates to achieve a complete perspective for the envisaged industry.

The data resulted from contact angle measurements (Table 6) were used to assess the wettability of both the plain biobased epoxy matrix (*E*) and GO of MMT-based nanocomposite coatings. The results of neat biobased epoxy coatings with a CA of 94° indicate that they are more hydrophobic than conventional epoxy networks, which have a CA around 74° according to literature data[41] due to the triglyceride backbone of ELO. However, the nanocomposite coatings possess lower CA values, generated on one hand by the OH functionalities from epoxy ring opening in the curing reaction, and by the functional groups from the nanoreinforcing agents on the other hand. Despite this aspect, the compatibility with the matrix for the reinforcing agents can be given by the closest value of water CA to the one presented by the ELO matrix (as highlighted by bold values in Table 6).

Table 6. Contact Angle and Antibacterial Activity Data for the ELO-Based Nanocomposites

sample	report (%)	CA (deg) water	CA (deg) EG	surface free energy (Nm/m)	CFU/mL
E		94.25	67.49	29.50	3×10^8
EG	0.25	**92.81**	73.12	20.80	1×10^8
	0.5	87.64	65.67	24.88	
	1	87.10	67.81	22.84	
EGD	0.25	75.14	56.89	29.12	2×10^8
	0.5	**93.66**	71.04	23.70	
	1	91.37	68.67	24.45	
EM	0.25	89.27	69.02	22.67	5×10^6
	0.5	**92.13**	67.35	26.89	
	1	89.15	64.68	27.27	
EMD	0.25	84.39	70.82	21.99	4×10^7
	0.5	88.95	66.73	24.67	
	1	**93.63**	68.75	26.73	

Furthermore, the chemical composition of the polymeric nanocomposites plays an important role in the surface energy values measured on the exposed surface but with high importance to adhesion to different substrates. A lower surface energy given by the good dispersion and increased surface roughness caused by embedding of the GO and MMT nanofillers into the polymeric matrix will enable a broader application toward designing an intelligent surface adhesion management system. In the case of nanocomposites reinforced with MMT structures, one can observe that this parameter increases proportionally with the concentration of the filler. By addition of 1% nanoclay, surface free energy is similar to the one recorded for the ELO matrix, suggesting a lower interaction between the two components of the system, as also proven by the DMA results.

It is well known that materials with surface free energy around 20 Nm/m are compatible with hydrophobic substrates such as Teflon;[42] this aspect encourages a widening of the perspectives for different antibacterial applications of the developed materials. Based on this hypothesis, the intrinsic antimicrobial activity of 0.25% ELO-based nanocomposites was evaluated and the results are compiled in Table 6. The antibacterial activity of the GO, GOD, MMT, and MMTD nanostructures was tested against *Staphylococcus aureus* bacterial strains, and the results suggest a significant decrease of CFU on the coatings. A 2 magnitude order lower CFU for MMT demonstrated that it can act as a biocide, without additional expensive and toxic antimicrobial agents such as fluoride[43] and polyhexamethylene guanidine molybdate[44] and metal nanoparticles[45] such as copper[46] or silver.[47]

3.6. Swelling Degree (SD). For a deeper understanding of the ELO-based networks, a series of SD monitoring in common epoxy usage media was carried out, and the corresponding results can be observed in Figure 5. In most cases, the stronger the cross-linked networks, the lower the SD should be obtained. This fact is appliable in the case of water uptake when the cross-linking density variations are well correlated with the SD values as the nanocomposites reinforced with GO structures have a higher average uptake. Nevertheless, these values are still lower than the cured matrix because of the physical interactions and steric hindrance exerted by the GO sheets. However, in this study, we showed that complex interactions between functional groups of the nanoreinforcing agents could lead to a disruption in linear

https://doi.org/10.1021/acsomega.3c09059
ACS Omega 2024, 9, 8297−8307

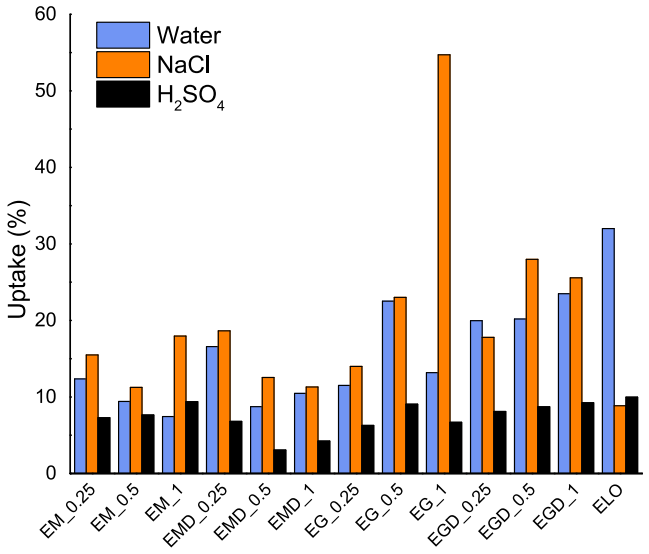

Figure 5. Swelling degrees for biobased ELO nanocomposites in different media.

behavior. When the SD was measured in NaCl solution, the electrostatic forces generated by functional groups exerted a larger influence on the uptake values, thus giving information about surface and edge exposure also. A maximum NaCl uptake of 52% was noticed for 1% GO composites, which can be assigned to a plateau level of GO sheet distribution, leading to an agglomerated reinforcing agent, which further disrupts epoxy network formation.

3.7. Morphology and Dispersion Estimation. The fracture morphology for the nanocomposite systems was evaluated through SEM and the corresponding images are presented in Figure 6. The difference between the morphology of the graphene oxide flakes and stacked layers of nanoclay leads to a contrast in the surface contact between the two phases and subsequently leads to a better transfer of structural and thermomechanical properties. To gain a better understanding of the influence exerted by these nanostructures, 1% formulations were analyzed. A homogeneous distribution of the nanoparticles within the epoxy network strongly influences the overall performance of the coatings both as thermal characteristics and wearability.[38,48]

Looking at the surface fracture of the neat GO- and MMT-based nanocomposites, it can be seen that a similar roughness is obtained. This demonstrated that the rigid nanostructures have a lower compatibility with ELO in comparison to the functionalized ones. The additional amino functionalities participate in the curing process by developing efficient network interactions that translate into a smooth homogeneous fracture, as also highlighted by the curing enthalpy data. Furthermore, the previous statement is sustained by the embedded reinforcing agents pointed out in Figure 6, EGD_1 and EMD_1.

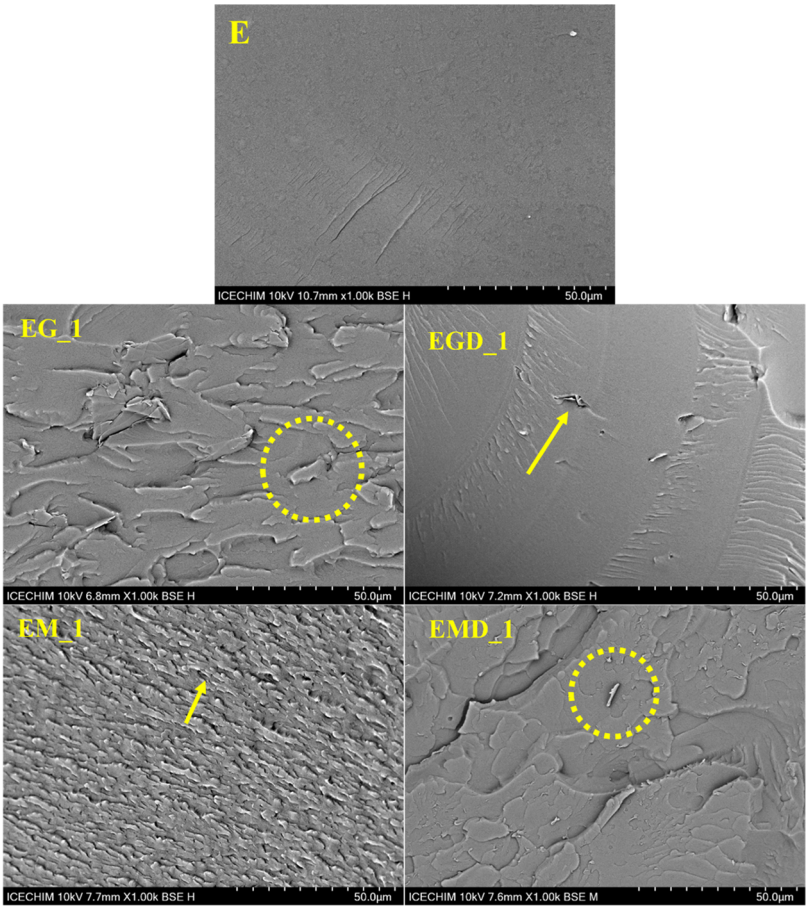

Figure 6. SEM micrographs of neat ELO and ELO-based nanocomposites with 1% nanoreinforcing agent.

https://doi.org/10.1021/acsomega.3c09059
ACS Omega 2024, 9, 8297−8307

4. CONCLUSIONS

Sustainable epoxy networks were designed with improved thermal and mechanical properties, intended for coating applications. A complex calorimetric study, which combined the analysis of MMT and GO nanoreinforcing agents on the curing enthalpy, along with the cure rate given by the topochemistry enhanced by their functional groups, led to valuable findings regarding the efficient formation of ELO networks with lower E_a values and higher cross-linking densities.

The type and concentration of each nanoreinforcing agent such as GO and MMT used for the development of the nanocomposite materials have a significant influence upon the overall properties. The presence of the additional amino groups in the functionalized nanostructures facilitates the epoxy ring opening reactions along with the formation of ester bonds, thus generating increased values for the curing enthalpy. The lower values for the E_a computed for the curing reaction of the EGD and EGM nanocomposites correlate with the DSC results, thus suggesting a synergistic effect of the nanohybrid structures over the curing process.

In the case of the viscoelastic properties of the MMT nanocomposites, the decreased values for the T_g represent a consequence of the agglomeration of the nanoclay. GO and GOD demonstrate an increased compatibility with the polymeric matrix, as suggested by the higher values for the T_g and E'.

The thermal properties of the nanocomposite materials were altered by the presence of the reinforcing agents, as suggested by the char yield and the onset of thermal degradation ($T_{d3\%}$). The degradation mechanism may be influenced by the additional interactions between the ELO matrix and the surface of the nanohybrid structures.

Surface properties revealed that the nanocomposite materials are less hydrophobic than the neat ELO matrix mainly due to the presence of polar OH groups formed during the epoxy ring opening reaction and the nanoreinforcing agents. The surface free energy is strongly influenced by the morphology and distribution of the filler within the matrix and also suggests promising potential for further applications in antibacterial coatings. The results of the swelling degree analysis demonstrate a complex interaction between the ELO matrix and the functional groups of the nanohybrid structures; thus, the expected linear behavior is strongly affected by possible electrostatic interactions in the case of NaCl solution. Fracture morphology reveals that neat GO and MMT have a lower compatibility with the polymeric matrix, while functionalized nanoreinforcing agents lead to a smoother and more homogeneous fracture surface.

ASSOCIATED CONTENT

Supporting Information

The Supporting Information is available free of charge at https://pubs.acs.org/doi/10.1021/acsomega.3c09059.

Thermal stability curves for ELO-based nanocomposites in air, as shown in Figure S1; derivative thermal stability curves for ELO-based nanocomposites in air, as depicted in Figure S2 (PDF)

AUTHOR INFORMATION

Corresponding Author

Celina Maria Damian − *Advanced Polymer Materials Group, National University of Science and Technology Politehnica Bucharest, Bucharest 011061, Romania;* orcid.org/0000-0001-6109-6630; Email: celina.damian@upb.ro

Authors

Mădălina Ioana Necolau − *Advanced Polymer Materials Group, National University of Science and Technology Politehnica Bucharest, Bucharest 011061, Romania*

Brînduşa Bălănucă − *Advanced Polymer Materials Group, National University of Science and Technology Politehnica Bucharest, Bucharest 011061, Romania; Department of Organic Chemistry "C. Nenitescu", National University of Science and Technology Politehnica Bucharest, Bucharest 011061, Romania*

Adriana Nicoleta Frone − *National Institute for Research & Development in Chemistry and Petrochemistry − ICECHIM, Bucharest 060021, Romania;* orcid.org/0000-0001-6232-886X

Iulia Nicoleta Radu − *Advanced Polymer Materials Group, National University of Science and Technology Politehnica Bucharest, Bucharest 011061, Romania*

Graţiela Grădişteanu-Pîrcălăbioru − *eBio-hub Research-Center, National University of Science and Technology Politehnica Bucharest, Bucharest 061344, Romania; Research Institute of University of Bucharest, University of Bucharest, Bucharest 050095, Romania; Academy of Romanian Scientists, Bucharest 050094, Romania*

Complete contact information is available at: https://pubs.acs.org/10.1021/acsomega.3c09059

Notes

The authors declare no competing financial interest.

ACKNOWLEDGMENTS

The research work was funded by a grant of the Romanian Ministry of Education and Research, CNS-UEFISCDI, through project number TE48/2022, project code PN-III-P1-1.1-TE-2021-0627: "Sustainable epoxy networks with tunable properties used as nanocomposite materials for coatings" (GREEN-NanoNET). The Open Access publication charges were granted by the National University of Science and Technology Politehnica through the PubArt project. The contact angle measurements were possible due to the European Regional Development Fund through the Competitiveness Operational Program 2014−2020, priority axis 1, project number P_36_611, MySMIS code 107066: Innovative Technologies for Materials Quality Assurance in Health, Energy and Environmental Center for Innovative Manufacturing Solutions of Smart Biomaterials and Biomedical Surfaces (INOVA-BIOMED).

REFERENCES

(1) Massingill, J. L.; Bauer, R. S. Epoxy Resins. In *Applied Polymer Science: 21st Century*; Craver, C. D.; Carraher, C. E., Eds.; Pergamon: Oxford, 2000; pp 393−424.

(2) Jelić, A.; Sekulić, M.; Travica, M.; Gržetić, J.; Ugrinović, V.; Marinković, A. D.; Božić, A.; Stamenović, M.; Putić, S. Determination of Mechanical Properties of Epoxy Composite Materials Reinforced with Silicate Nanofillers Using Digital Image Correlation (DIC). *Polymers* **2022**, *14*, 1255.

(3) Huang, Y.; Tian, Y.; Li, Y.; Tan, X.; Li, Q.; Cheng, J.; Zhang, J. High mechanical properties of epoxy networks with dangling chains and tunable microphase separation structure. *RSC Adv.* **2017**, *7*, 49074−49082.
(4) Lee, J. W.; Kim, S.-S.; Lee, M. W.; Hwang, J. Y.; Moon, S. Y. High-Strength Epoxy Nanocomposites Reinforced with Photochemically Treated CNTs. *ACS Omega* **2023**, *8*, 19789−19797.
(5) Białkowska, A.; Bakar, M.; Kucharczyk, W.; Zarzyka, I. Hybrid Epoxy Nanocomposites: Improvement in Mechanical Properties and Toughening Mechanisms-A Review. *Polymers* **2023**, *15*, 1398.
(6) Dideikin, A. T.; Vul', A. Y. Graphene Oxide and Derivatives: The Place in Graphene Family. *Front. Phys.* **2019**, *6*, No. 149.
(7) Smith, A. T.; LaChance, A. M.; Zeng, S.; Liu, B.; Sun, L. Synthesis, properties, and applications of graphene oxide/reduced graphene oxide and their nanocomposites. *Nano Mater. Sci.* **2019**, *1*, 31−47.
(8) Jiříčková, A.; Jankovský, O.; Sofer, Z.; Sedmidubský, D. Synthesis and Applications of Graphene Oxide. *Materials* **2022**, *15*, 920.
(9) Lee, S. J.; Yoon, S. J.; Jeon, I.-Y. Graphene/Polymer Nanocomposites: Preparation, Mechanical Properties, and Application. *Polymers* **2022**, *14*, 4733.
(10) Kumar, S. S. A.; Bashir, S.; Ramesh, K.; Ramesh, S. New perspectives on Graphene/Graphene oxide based polymer nanocomposites for corrosion applications: The relevance of the Graphene/Polymer barrier coatings. *Prog. Org. Coat.* **2021**, *154*, No. 106215.
(11) Fu, X.; Lin, J.; Liang, Z.; Yao, R.; Wu, W.; Fang, Z.; Zou, W.; Wu, Z.; Ning, H.; Peng, J. Graphene oxide as a promising nanofiller for polymer composite. *Surf. Interfaces* **2023**, *37*, No. 102747.
(12) Abulyazied, D. E.; Ene, A. An Investigative Study on the Progress of Nanoclay-Reinforced Polymers: Preparation, Properties, and Applications: A Review. *Polymers* **2021**, *13*, 4401.
(13) Guo, F.; Aryana, S.; Han, Y.; Jiao, Y. A Review of the Synthesis and Applications of Polymer−Nanoclay Composites. *Appl. Sci.* **2018**, *8*, 1696.
(14) Azeez, A. A.; Rhee, K. Y.; Park, S. J.; Hui, D. Epoxy clay nanocomposites − processing, properties and applications: A review. *Composites, Part B* **2013**, *45*, 308−320.
(15) Adekunle, K. F. A Review of Vegetable Oil-Based Polymers: Synthesis and Applications. *Open J. Polym. Chem.* **2015**, *05* (03), 34.
(16) Oyman, Z. O.; Ming, W.; Linde, R.v.d. Oxidation of drying oils containing non-conjugated and conjugated double bonds catalyzed by a cobalt catalyst. *Prog. Org. Coat.* **2005**, *54*, 198−204.
(17) Karak, N. Vegetable Oils and Their Derivatives. In *Vegetable Oil-Based Polymers*; Karak, N., Ed.; Woodhead Publishing, 2012; Chapter 3, pp 54−95.
(18) Sahoo, S. K.; Khandelwal, V.; Manik, G. Development of completely bio-based epoxy networks derived from epoxidized linseed and castor oil cured with citric acid. *Polym. Adv. Technol.* **2018**, *29*, 2080−2090.
(19) Petrović, Z. S.; Hong, J.; Vuković, M. L.; Djonlagić, J. Epoxy resins and composites from epoxidized linseed oil copolymers with cyclohexene oxide. *Biocatal. Agric. Biotechnol.* **2022**, *39*, No. 102269.
(20) Yang, J.; Dong, X.; Wang, J.; Ching, Y. C.; Liu, J.; Chunhui, l.; Baikeli, Y.; Li, Z.; Mohammed Al-Hada, N.; Xu, S. Synthesis and properties of bioplastics from corn starch and citric acid-epoxidized soybean oil oligomers. *J. Mater. Res. Technol.* **2022**, *20*, 373−380.
(21) Silva, R. S.; Maia, D. L. H.; Fernandes, F. A. N. Production of tung oil epoxy resin using low frequency high power ultrasound. *Ultrason. Sonochem.* **2021**, *79*, No. 105765.
(22) Gaina, C.; Ursache, O.; Gaina, V.; Serban, A. M.; Asandulesa, M. Novel Bio-Based Materials: From Castor Oil to Epoxy Resins for Engineering Applications. *Materials* **2023**, *16*, 5649.
(23) Madhusudhana, A. M.; Mohana, K. N. S.; Hegde, M. B.; Nayak, S. R.; Rajitha, K.; Sunil Kumar, M. C. Functionalized graphene oxide dispersed polyvinyl alcohol-epoxidized linseed oil composite: An eco-friendly and promising anticorrosion coating material. *Colloids Surf., A* **2022**, *650*, No. 129382.
(24) Alam, J.; Alam, M.; Raja, M.; Abduljaleel, Z.; Dass, L. A. MWCNTs-Reinforced Epoxidized Linseed Oil Plasticized Polylactic Acid Nanocomposite and Its Electroactive Shape Memory Behaviour. *Int. J. Mol. Sci.* **2014**, *15*, 19924−19937.
(25) Lligadas, G.; Ronda, J. C.; Galià, M.; Cádiz, V. Bionanocomposites from Renewable Resources: Epoxidized Linseed Oil−Polyhedral Oligomeric Silsesquioxanes Hybrid Materials. *Biomacromolecules* **2006**, *7*, 3521−3526.
(26) Kumar, S.; Mohanty, S.; Nayak, S. K. Nanocomposites of epoxidized soybean oil (ESO)-based epoxy (DGEBA) blends and clay platelets: cured with methylhexahydrophthalic anhydride crosslinker. *J. Macromol. Sci., Part A* **2020**, *57*, 654−662.
(27) Hegde, M. B.; Mohana, K. N. S.; Rajitha, K.; Madhusudhana, A. M. Reduced graphene oxide-epoxidized linseed oil nanocomposite: A highly efficient bio-based anti-corrosion coating material for mild steel. *Prog. Org. Coat.* **2021**, *159*, No. 106399.
(28) Balanuca, B.; Raluca, S.; Hanganu, A.; Iovu, H. Novel linseed oil-based monomers: Synthesis and characterization. *UPB Sci. Bull., Ser. B: Chem. Mater. Sci.* **2014**, *76*, 129−140.
(29) Necolau, M. I.; Damian, C. M.; Fierăscu, R. C.; Chiriac, A.-L.; Vlăsceanu, G. M.; Vasile, E.; Iovu, H. Layered Clay−Graphene Oxide Nanohybrids for the Reinforcement and Fire-Retardant Properties of Polyurea Matrix. *Polymers* **2022**, *14*, 66.
(30) Hardis, R.; Jessop, J. L. P.; Peters, F. E.; Kessler, M. R. Cure kinetics characterization and monitoring of an epoxy resin using DSC, Raman spectroscopy, and DEA. *Composites, Part A* **2013**, *49*, 100−108.
(31) Lascano, D.; Lerma-Canto, A.; Fombuena, V.; Balart, R.; Montanes, N.; Quiles-Carrillo, L. Kinetic Analysis of the Curing Process of Biobased Epoxy Resin from Epoxidized Linseed Oil by Dynamic Differential Scanning Calorimetry. *Polymers* **2021**, *13*, 1279.
(32) Kim, T. H.; Kim, M.; Lee, W.; Kim, H.-G.; Lim, C.; Seo, B. Synthesis and Characterization of a Polyurethane Phase Separated to Nano Size in an Epoxy Polymer. *Coatings* **2019**, *9*, 319.
(33) Senthilkumar, R.; Natarajan, M. P.; Ponnuvel, S.; Sathyamurthy, R. Mechanical and visco elastic analysis of Sal tree gum incorporated epoxy bio composite. *J. Mater. Res. Technol.* **2022**, *17*, 819−827.
(34) Khandelwal, V.; Sahoo, S. K.; Kumar, A.; Sethi, S. K.; Manik, G. Bio-sourced electrically conductive epoxidized linseed oil based composites filled with polyaniline and carbon nanotubes. *Composites, Part B* **2019**, *172*, 76−82.
(35) Suthar, V.; Asare, M. A.; de Souza, F. M.; Gupta, R. K. Effect of Graphene Oxide and Reduced Graphene Oxide on the Properties of Sunflower Oil-Based Polyurethane Films. *Polymers* **2022**, *14*, 4974.
(36) Prashantha, K.; Schmitt, H.; Lacrampe, M. F.; Krawczak, P. In *Processing and Mechanical Behaviour of Halloysite Filled Polyamide-6 Nanocomposites*, 18th International Conference on Composite Materials, 2011.
(37) Díez-Pascual, A. M.; Díez-Vicente, A. L. Development of linseed oil−TiO2 green nanocomposites as antimicrobial coatings. *J. Mater. Chem. B* **2015**, *3*, 4458−4471.
(38) Feichtenschlager, B.; Pabisch, S.; Svehla, J.; Peterlik, H.; Sajjad, M.; Koch, T.; Kickelbick, G. Epoxy Resin Nanocomposites: The Influence of Interface Modification on the Dispersion Structure—A Small-Angle-X-ray-Scattering Study. *Surfaces* **2020**, *3*, 664−682.
(39) Yazman, Ş.; Uyaner, M.; Karabörk, F.; Akdemir, A. Effects of nano reinforcing/matrix interaction on chemical, thermal and mechanical properties of epoxy nanocomposites. *J. Compos. Mater.* **2021**, *55*, 4257−4272.
(40) Mendes, C.; Costa, P.; Roppolo, I.; Sangermano, M.; Lanceros-Méndez, S. Bio-based Piezo- and Thermo-Resistive Photo-Curable Sensing Materials from Acrylated Epoxidized Soybean Oil. *Macromol. Mater. Eng.* **2022**, *307*, No. 2100934.
(41) Khobragade, P.; Hansora, D.; Naik, J.; Njuguna, J.; Mishra, S. Physico-mechanical properties of nano polystyrene (nPS) decorated graphene oxide (GO) -epoxy composites. *Polym. Int.* **2017**, *66*, 1402.
(42) Selvakumar, N.; Barshilia, H. C.; Rajam, K. S. Effect of substrate roughness on the apparent surface free energy of sputter deposited

https://doi.org/10.1021/acsomega.3c09059
ACS Omega 2024, 9, 8297−8307

superhydrophobic polytetrafluoroethylene coatings: A comparison of experimental data with different theoretical models. *J. Appl. Phys.* **2010**, *108*, No. 013505.
(43) Breaker, R. R. New Insight on the Response of Bacteria to Fluoride. *Caries Res.* **2012**, *46*, 78−81.
(44) Zhang, T.; Wan, H.; Xu, Z.; Zhang, Y.; Dai, J.; Liu, H. Polyhexamethylene guanidine molybdate as an efficient antibacterial filler in epoxy coating for inhibiting sulfate reducing bacteria biofilm. *Prog. Org. Coat.* **2023**, *176*, No. 107401.
(45) Samardžija, M.; Stojanović, I.; Domanovac, M. V.; Alar, V. Epoxy Coating Modification with Metal Nanoparticles to Improve the Anticorrosion, Migration, and Antibacterial Properties. *Coatings* **2023**, *13*, 1201.
(46) Das, G.; Kalita, R. D.; Gogoi, P.; Buragohain, A. K.; Karak, N. Antibacterial activities of copper nanoparticle-decorated organically modified montmorillonite/epoxy nanocomposites. *Appl. Clay Sci.* **2014**, *90*, 18−26.
(47) Roy, B.; Bharali, P.; Konwar, B. K.; Karak, N. Silver-embedded modified hyperbranched epoxy/clay nanocomposites as antibacterial materials. *Bioresour. Technol.* **2013**, *127*, 175−180.
(48) Karbowniczek, J. E.; Ura, D. P.; Stachewicz, U. Nanoparticles distribution and agglomeration analysis in electrospun fiber based composites for desired mechanical performance of poly(3-hydroxybuty-rate-co-3-hydroxyvalerate (PHBV) scaffolds with hydroxyapatite (HA) and titanium dioxide (TiO2) towards medical applications. *Composites, Part B* **2022**, *241*, No. 110011.

https://doi.org/10.1021/acsomega.3c09059
ACS Omega 2024, 9, 8297−8307